

Article

Wireless Magnetoelasticity-Based Sensor for Monitoring the Degradation Behavior of Polylactic Acid Artificial Bone In Vitro

Kun Yu , Limin Ren , Yisong Tan *  and Junyao Wang

School of mechanical engineering, Northeast electric power University, Jilin 132000, China; 2201700350@neepu.edu.cn (K.Y.); renlimin@neepu.edu.cn (L.R.); junyao_0001@neepu.edu.cn (J.W.)

* Correspondence: tanyisong@neepu.edu.cn; Tel.: +86-432-6480-7382

Received: 23 January 2019; Accepted: 17 February 2019; Published: 20 February 2019



Abstract: A magnetoelasticity-based (MB) sensor was employed for monitoring the degradation behavior of polylactic acid (PLA) artificial bone (PAB) in vitro, which can be used as an implant to repair bone defects. Biodegradable PLA material was coated on both sides of the MB sensor strip with a 3D printer, forming PAB. The PAB samples were submerged in an alkaline medium (pH = 12) and a neutral phosphate-buffered saline (PBS) medium (pH = 7.4). The degradation behavior of the PAB was monitored wirelessly based on changes in the output power of the MB sensor. The results indicated that the output power varied by almost 0.2 and 0.11 dbm over 15 days in the two media. The degradation behavior monitored by the MB sensor agreed with the theoretical analysis. The MB sensor provides a wireless method for monitoring the degradation behavior of PAB in vitro and requires few samples at a lower cost. Importantly, the results showed that biological tissues had almost no effect on the monitoring function of the MB sensor. Therefore, the MB sensor technology is highly attractive for fully characterizing the degradation behavior of bone implants in a larger range of physiological conditions, and will be applied to monitor the degradation behavior in vivo.

Keywords: magnetoelasticity-based sensor (MB sensor); polylactic acid (PLA) artificial bone (PAB); theoretical analysis; degradation behavior in vitro

1. Introduction

Bioabsorbable or biodegradable bone defect repair devices made of synthetic polymer have been used as alternative bioappliances for the internal repair of bone defects, particularly those in load-bearing bone. The overall results so far have been encouraging [1,2]. There are some merits to using bioabsorbable or biodegradable bone defect repair devices: there is no need to remove the device after the bone defect heals, in contrast to metal fixation devices [3]; and using bioabsorbable implants prevents the stress-shielding atrophy and weakening of the fixed bone that is usually caused by rigid metallic fixation [4]. However, the prolonged presence of an implant can act as a barrier for new bone regeneration. Thus, the degradation behavior of an implant must be tailored to match the bone ingrowth as the bone defect heals.

Recently, polylactic acid (PLA) has been recognized as a biodegradable polymer material and used in a number of biomedical applications, including sutures, pins, screws [5,6], scaffolds, drug delivery, and internal repair devices [7]. PLA has good mechanical properties paired with biocompatibility, and can be used to fabricate biodegradable products that are naturally metabolized in vivo to yield carbon dioxide and water [8]. PLA has been tested as a replacement material for prostheses because of its high strength performance [9,10]. Many studies have been carried out on its hydrolytic degradation in different media, including a neutral solution of phosphate-buffered saline (PBS) at 37 °C or higher to

accelerate degradation [11], an alkaline solution at different temperatures [12], and an acid solution [13]. There have even been studies on its enzymatic degradation with enzymes such as proteinase K [14].

While the pH of internal organs ranges from 7.2 to 7.45 [15], the pH levels of skin (pH = 4–6) [16], subcutaneous tissues (pH = 6.7–7.1) [17], tumors (pH < 6.9) [18], and internal tissues prolonged hemorrhaging (pH < 7) [19] are more acidic. Therefore, the degradation behavior of PLA artificial bone (PAB) needs to be characterized under multiple conditions to better mimic the various physiological environments. Importantly, the different pH media can cause different corrosion conditions in PAB. Hence, an alkaline medium (pH = 12) and a neutral PBS solution medium (pH = 7.4) are used to degrade the PAB. However, the traditional methods [11,12], such as weight loss, observe the surface characteristics by scanning electron microscope (SEM) and thermal analysis, and can only be used in vitro to assess the degradation condition, and require a great deal of samples at a high cost. If PAB is implanted in vivo, all traditional methods lose their efficacy. Hence, the magnetoelasticity-based (MB) sensor presented in our study is employed to monitor the degradation behavior.

Magnetoelasticity-based sensors have been used to track the degradation behavior of bioadhesives over a period of time [20]. The ability to wirelessly monitor changes in permeability allows the Magnetoelasticity-Based (MB) sensors to be applied to monitoring stress in bone plates [21] and the tensile force of sutured wound sites [22]. Fortunately, the permeability of MB sensors is sensitive to compressive and tensile stresses. Hence, wireless MB sensors are applied to monitor the degradation behavior of PAB based on the relationship between output power of the MB sensor and external compressive force with the degradation of the PAB.

In this study, an MB sensor was used to monitor the degradation behavior of PAB in vitro. PAB was fabricated by coating both sides of an MB sensor with PLA using a 3D printer. PAB samples were subjected to the hydrolytic degradation process in PBS (pH = 7.4) and NaOH (pH = 12) media over 15 days at body temperature (37 °C). PAB was tested with a self-developed experimental platform every 7 days, and the changes in permeability of the MB sensor were tracked wirelessly. The varying permeability can reflect the degradation behavior of the PAB, and is supported by theoretical analysis. The changes in the weight and volume of PAB were also measured with traditional methods and a scanning electronic microscope (SEM).

2. Materials and Methods

2.1. Theoretical Analysis of the Magnetoelasticity-Based (MB) Sensor

The MB sensor [23,24] (Metglas 2826 MB, Hong Kong, China) was purchased from Hong Kong, China, as a continuous ribbon of 11.7 mm width and 28 μm thickness containing 40% Fe, 38% Ni, 18% B, and 4% Mo ($\text{Fe}_{40}\text{Ni}_{38}\text{Mo}_4\text{B}_{18}$). The magnetoelastic coupling factor reached 0.98 and a magnetostriction of 12×10^{-6} [25,26]. The physical and magnetic properties of the material are presented in Table 1. This material has special characteristics such as low resistivity, high permeability, and a high magnetoelastic coefficient, and is much thinner and cheaper than Terfenol-D and galfenol, which gives it a wide range of applications [27]. The principle is based on the inverse magnetoelastic effect (Villari effect)—when an MB sensor is subjected to tensile or compressive stress under an external magnetic field, its permeability changes accordingly. The variation in the permeability can cause a change in spatial magnetic field.

Magnetoelasticity refers to the coupling of magnetic and elastic/mechanical energies within a material. For the MB sensor, the reverse situation (i.e., Villari effect) also holds true in this study because an applied stress changes the susceptibility χ [26,28,29]:

$$\sigma = \frac{F}{A}, \quad (1)$$

$$\chi = \frac{M_s^2}{2KU - 3\lambda_s\sigma}. \quad (2)$$

Here, σ is the stress, F is the external force (50 and 100 N in this study), A is the force area of PAB, M_s is the magnetization density, K is the surface current density (current per unit length), U is the internal energy, λ_s is the saturation magnetostriction, and χ is the susceptibility.

Table 1. The magnetic and physical properties of magnetoelastic material.

Magnetic Properties		Physical Properties	
Saturation induction (T)	0.88	Density (g/cm ³)	7.90
Maximum D.C. permeability (μ):		Vicker's hardness (50 g load)	740
Annealed	800,000	Elastic modulus (GPa)	100–110
As-cast	>50,000	Tensile strength (GPa)	1–2
Saturation magnetostriction (ppm)	11.7	Lamination factor (%)	>75
Electrical resistivity ($\mu\Omega\cdot\text{cm}$)	138	Continuous service temperature. (°C)	125
Curie temperature (°C)	353	Thermal expansion (ppm/°C)	11.7
-	-	Crystallization temperature (°C)	410

The susceptibility of the material is directly related to its magnetic permeability by [26]

$$\mu = \mu_0(1 + \chi), \quad (3)$$

where μ is the permeability, and μ_0 is the vacuum permeability.

In this study, the stress (σ) of compressive force working on the MB sensor causes a change in the permeability (μ). Moreover, the degradation of PAB can cause a change in the force area of PAB (A), and then lead to the change in stress (σ). Hence, the relationship between degradation behavior of the PAB and the output power of the MB sensor was obtained to express the degradation behavior of the PAB in vitro. The Villari effect describes the magnetization change induced by a mechanical load. The response of the flux density with respect to the input stress is the principle of the MB sensor, as shown in Figure 1. Importantly, the stress range between phase M and phase N in Figure 1 was allocated to monitor the degradation behavior of PAB in this study.

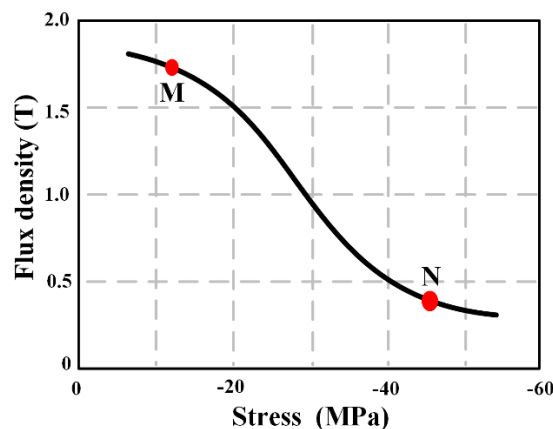


Figure 1. Sensing responses of a highly textured material under decreasing stress [30], expressed as the stress–flux density response.

2.2. Fabrication of the PLA artificial bone (PAB)-Coated MB Sensor

PLA (True Yellow, MakerBot Industries, USA) was coated on both sides of the MB sensor to form PAB with a 3D printer. The sample was fabricated based on the height gap between the layer thickness (0.3 mm) of the 3D printer and the thickness of the magnetoelastic sensor strip (28 μm). Pro/Engineering 4.0 was applied to design a PAB model (cylinder with a length of 25 mm and diameter of 15 mm). Then, it was printed with a MakerBot 3D printer (LLC One Metro Tech Centre, Brooklyn, USA). The MB sensor strip (20 mm \times 10 mm \times 28 μm) was embedded in the neutral surface of PAB with a quick adhesive (Gelianghao New Material Co., LTD, Shenyang, China). The thickness of the

sensor strip had little influence on the 3D printer. Hence, PAB could be fabricated with the 3D printer. The quick adhesive is not harmful to the human body, according to the Food and Drug Administration (FDA) of the USA and CE Marking of Europe [31]. The application of the PAB prototype is shown in Figure 2.

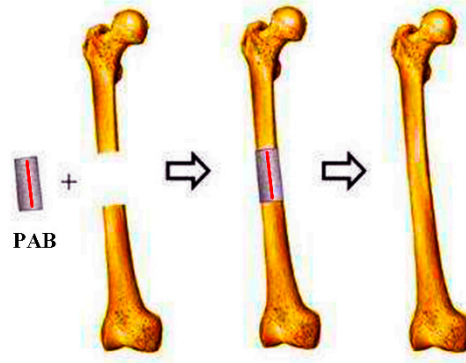


Figure 2. Poly-lactic acid (PLA) artificial bone (PAB) prototype applied to repair a bone defect (red line is the magnetoelasticity-based (MB) sensor).

2.3. Preparation of PAB Degradation

PAB samples were subjected to hydrolytic degradation at 37 °C for 15 days in two different media: a phosphate-buffered saline (PBS) solution with pH = 7.4 mimicking the internal conditions of humans and an NaOH solution with pH = 12 for an accelerated PAB degradation rate. The degradation media were renewed every 24 h. Five samples were prepared for those tests. All experiments were carried out in an incubator (37 °C /98.6 °F), and the degradation period was 15 days. Each sample was weighed with an electronic scale (KFS-C series, Kaifeng Inc. China) to obtain its initial mass (w_1).

2.4. Weight Loss of PAB

The weight loss was measured by immersing the PAB in PBS and alkaline solutions at 37 °C for 15 days. At the end of each time point, the samples were weighed after excess surface water was removed with filter paper. The weight loss (Q) of PAB was determined from the initial weight of the dry sample (w_1) and weight of the final dry sample (w_2):

$$Q(\%) = \frac{(w_1 - w_2)}{w_1} \times 100\%. \quad (4)$$

At the end of the predetermined time intervals (24 h), the samples were washed thoroughly with distilled water to eliminate any soluble inorganic salt and weighed after being completely vacuum-dried at 37 °C to obtain a constant weight for calculating the percentage of weight loss (Equation (4)).

2.5. Surface Characterization

The evolution of the PAB surface was evaluated with an SEM (Evo 18, Zeiss, Germany) at the beginning, middle, and end of the degradation time (i.e., days 0, 7, and 15) at different magnifications (500×, 5000×, 15,000×).

2.6. Monitoring the Degradation Behavior of PAB with the MB Sensor in Vitro

Figure 3 shows the experimental platform. PAB was fully fixed on the experimental platform and was compressed by the external force. It was surrounded by an exciting coil and a sensing coil. The outer coil comprised 0.5 mm diameter copper wire (line 25) with 200 turns and was used for excitation. It produced an alternating magnetic field (3×10^2 A/m) caused by a sinusoidal signal

(200 Hz and 2 V, peak to peak) and amplified by a power amplifier (TAPCO Juice™, Loud Technologies Inc. USA). The inner coil consisted of 0.25 mm diameter copper wire (line 33) with 200 turns and was used for sensing. It was connected with the spectrum analyzer to capture changes in the magnetic field. The results were stored in a computer for data analysis. In this study, the degradation of PAB caused a change in stress on the MB sensor, which led to the varying permeability. This change in the permeability of the MB sensor caused the change of the spatial magnetic field, which could be measured with the sensing coil. Therefore, the degradation of PAB was monitored by the MB sensor wirelessly. Importantly, no cables or batteries were needed for the MB sensor throughout the monitoring process.

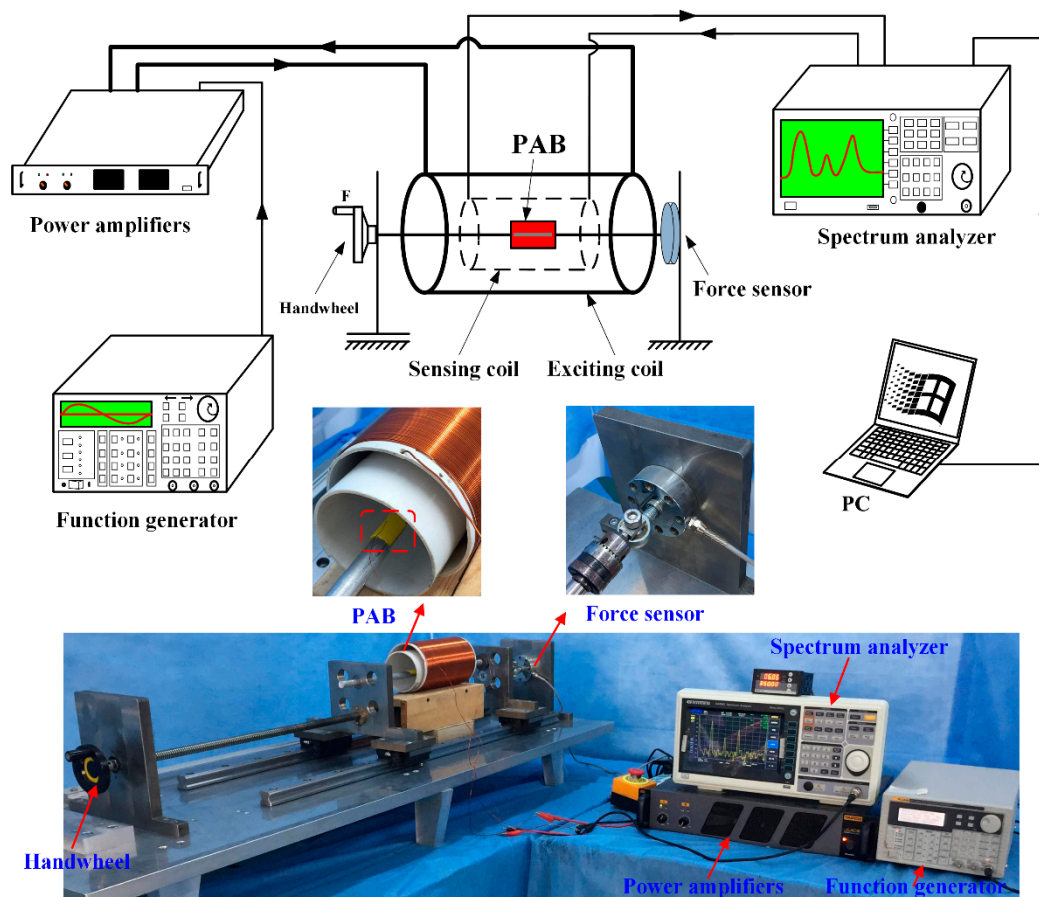


Figure 3. Experimental platform devices. The external compressive force (F) was applied on the PAB by the handwheel.

2.7. Simulated *In Vivo* Testing

PAB was implanted in a sheep leg to repair a bone defect, as shown in Figure 4. Then, the repaired sheep leg was tested with the experimental platform shown in Figure 3 after the implantation operation. This was a pre-experiment to verify the working condition of the MB sensor *in vivo*, and the effect of screws on the performance of the MB sensor was omitted in this study. The Ethics Committee at the Northeast Electric Power University Hospital has endorsed this study protocol according to the Code of Ethics of The World Medical Association (Declaration of Helsinki).

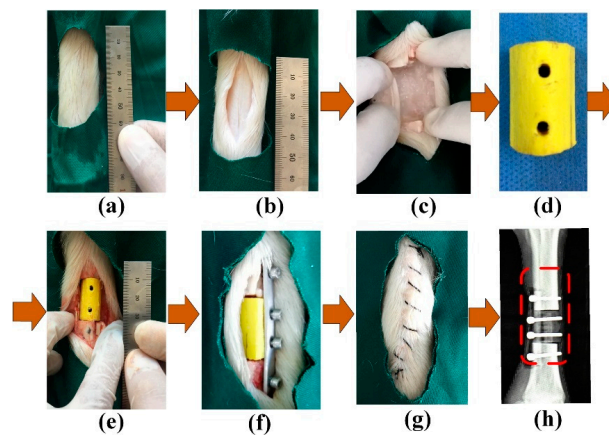


Figure 4. Implantation of the PAB: (a) sheep leg, (b) bone, (c) bone defect, (d) PAB, (e) implantation, (f) fixation, (g) suturing, and (h) X-ray image.

3. Results

3.1. Weight Loss of PAB

Figure 5 plots the weight loss of PAB in the PBS and NaOH media over 15 days. The weight loss decreased almost linearly and was faster in the alkaline medium than in the PBS medium. The weight variation trend of PAB was similar in the PBS and NaOH media. An average of 5 ± 0.1 g PLA was coated on the sensor strips. The 15 days of degradation produced losses of $2.5\% \pm 0.2\%$ and $6\% \pm 0.4\%$, respectively, of the original weight in the two media.

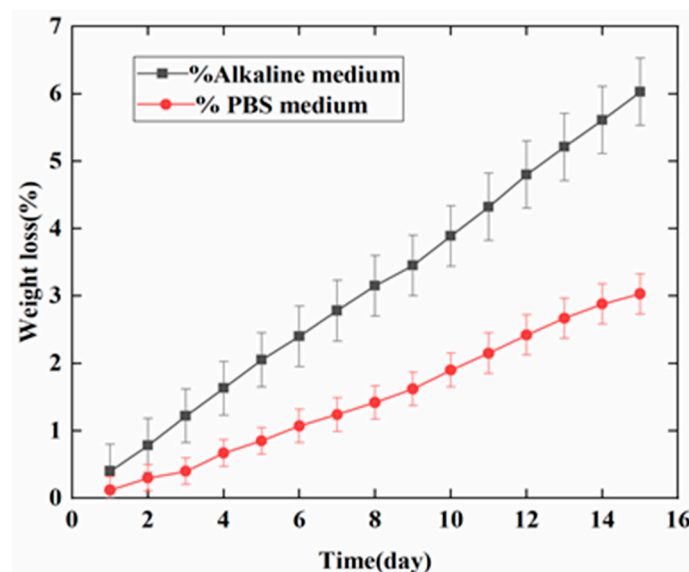


Figure 5. Weight loss of PAB in the alkaline and phosphate-buffered saline (PBS) media over 15 days.

3.2. Morphology of PAB

The morphology of PAB immersed in the NaOH medium was analyzed according to SEM images for days 0, 7, and 15, as shown in Figure 6. The surface of PAB before degradation (day 0) was smooth. After 15 days, PAB had a rougher appearance compared to days 0 and 7 at different magnifications ($500\times$, $5000\times$, $15,000\times$). The red circles in the SEM images indicate that the PAB degraded slowly in the NaOH medium at first. The degradation gradually increased on days 7 and 15. The images clearly show indications of PAB degradation.

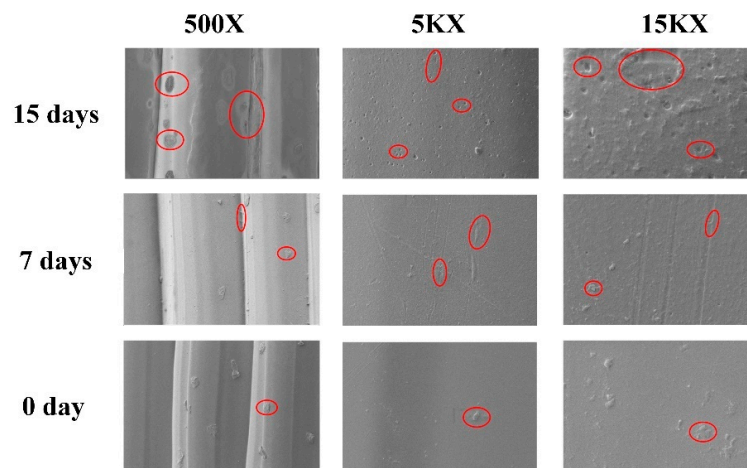


Figure 6. SEM images of PAB immersed in the NaOH medium at different magnifications (500 \times , 5000 \times , and 15,000 \times) and degradation times (days 0, 7, and 15). The red circles indicate the degradation condition of PAB.

3.3. MB Sensor Monitoring Results

Figure 7 indicates that the varying value of the output power increased with the external force (0–100 N) on PAB in vitro and in vivo (repaired the defect in the sheep leg). The maximum value was 0.04 dbm at 100 N. The increasing trend was similar both in vivo and in vitro. Figure 8 shows the variation of the output power when the external force was changed for the three days (days 0, 7, and 15) in the alkaline medium in vitro. Figure 8a indicates that the change of output power was low on day 0 in the alkaline medium at about 0.1 dbm. Importantly, the changes were about 0.15 dbm and 0.20 dbm on days 7 and 15, respectively. The output power gradually increased with degradation. Figure 8b further shows the increasing tendency of the output power at 10, 50, and 100 N on days 0, 7, and 15. Figure 9a shows the increasing output power in the PBS medium with values of 0.04, 0.07, and 0.1 dbm for days 0, 7, and 15, respectively. Figure 9b further shows the details of the output power at 10, 50, and 100 N. The variation of the output power of PAB in the alkaline medium was higher than that in PBS.

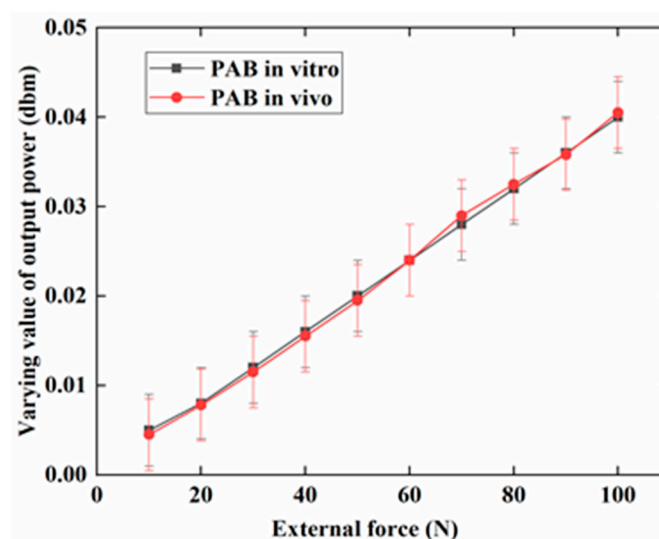


Figure 7. Varying values of the output power when an external force of 0–100 N was applied to PAB in vitro and in vivo (repaired sheep leg).

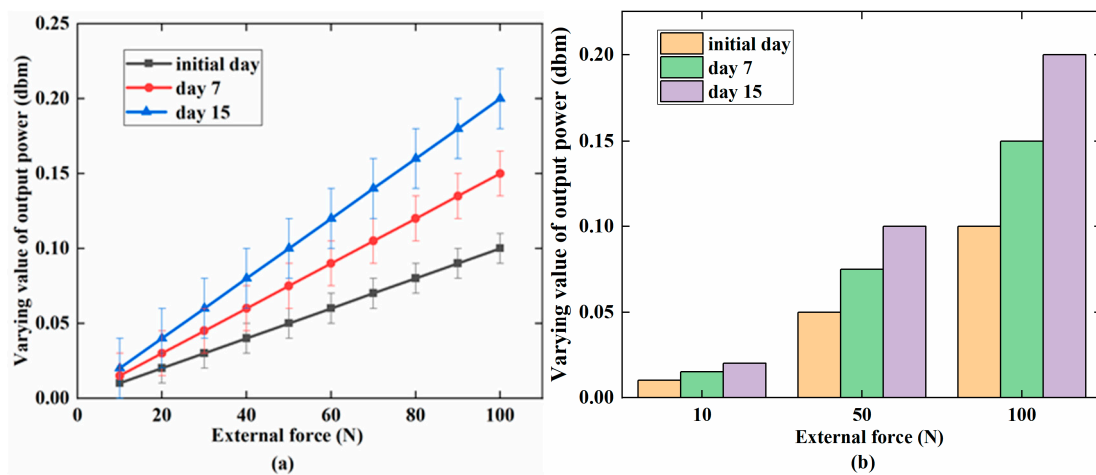


Figure 8. In the alkaline medium (pH = 12): (a) the linear increase in the varying value of the output power with an increasing external force (0–100 N) for the three phases; (b) the comparison of output power (dbm) for days 0, 7, and 15 at 10, 50, and 100 N.

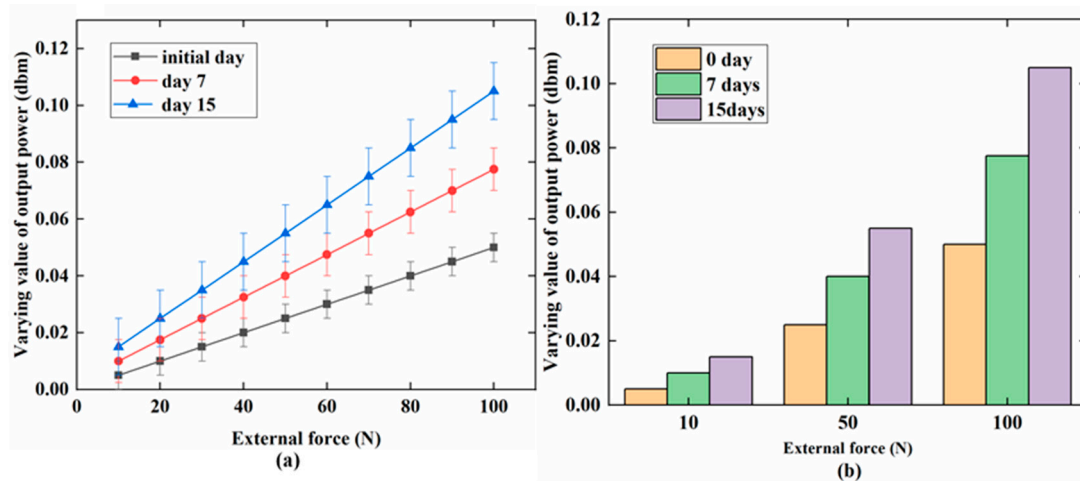


Figure 9. In the PBS medium (pH = 7.4): (a) a relationship between the varying value of the output power (dbm) and external force (N) on days 0, 7, and 15; (b) a detailed comparison of output power at 10, 50, and 100 N for the three days.

4. Discussion

The traditional PLA degradation measurement patterns (i.e., weight loss, morphological change) have been widely studied. However, this study was the first to use an MB sensor to monitor PAB degradation wirelessly and passively. In general, the results indicated that incorporating an MB sensor in PAB allowed the degradation behavior to be monitored *in vitro*. The *in vitro* weight loss and SEM monitoring of the PAB degradation behavior [32] were used to further elucidate the viability of the MB sensor. A theoretical analysis was also performed to verify the viability of using the MB sensor to monitor the degradation behavior of PAB.

About 5 ± 0.1 g of PLA was coated on the MB sensor strip. The PAB weight decreased by 0.3 ± 0.03 g in the alkaline medium and 0.15 ± 0.03 g in the PBS medium over 15 days. SEM images clearly showed the weight loss of PAB in the alkaline medium. In previous studies, Araque-Monros [33] used the traditional methods of weight loss, SEM micrographs, thermal analysis, and others to monitor the degradation process of a new PLA braided biomaterial, while Yuan et al [12] used the mass, morphology, thermal behavior, and tensile properties of PLA to monitor its surface degradation. The weight loss and SEM imaging results in this study were similar to those described in the above papers.

Figure 7 shows that the varying value of output power had the same trend when PAB was tested in vivo and in vitro. This indicates that biological tissues have almost no effect on the output power. Therefore, the MB sensor can be used in vivo to monitor the degradation behavior of bioimplants in the future.

Figures 8 and 9 present the varying values of the output power when PAB was incubated in alkaline (pH = 12) and PBS (pH = 7.4) media for 15 days. On day 0, the output power was lower than that on days 7 and 15. As the degradation time increased, more PLA degraded, and the diameter and weight of PAB were reduced. The external force could cause a large amount of stress on the MB sensor, which could increase its permeability. The output power of PAB with external forces of 10, 50, and 100 N was further studied for the three days, as shown in Figures 8b and 9b. The effect of degradation on the MB sensor at these specific forces was considered. The output power gradually increased from day 0 to day 7 and day 15, but the only difference was the increasing tendency. This can further explain the degradation behavior of the PAB. Thus, the MB sensor could monitor and reflect the degradation behavior under different conditions wirelessly and passively (i.e., medium and external force).

The output power shown in Figure 8a was higher than that shown in Figure 9a on days 0, 7, and 15. PAB degraded more quickly in the alkaline medium than in the PBS medium. The different degradation conditions led to different stresses working on the MB sensor. The different degradation conditions also caused different permeabilities in the MB sensor. Furthermore, the change in the PAB diameter could affect the permeability of the MB sensor in the same environment. In this study, the PAB diameter was 15 ± 0.05 mm at the beginning of degradation and decreased to 14.92 ± 0.02 mm in the alkaline medium and 14.96 ± 0.02 mm in the PBS medium over 15 days. Table 2 gives the variation of the PAB diameter in the two media over 15 days, and the varying value of the output power increased. The diameter and weight of PAB gradually decreased with increasing degradation time, as shown in Figure 10a. The output power increased with the degradation of PAB, as shown in Figure 10b.

Table 2. Relationship between the degradation time (days) and PAB condition under different immersion conditions.

Time (days) (PAB Condition)	0 (Without Treatment)	15 (In Alkaline Media)	15 (In PBS Media)
Diameter of PAB (mm)	15 ± 0.05	14.92 ± 0.02	14.96 ± 0.02
Weight loss (g)	0	0.3 ± 0.03	0.15 ± 0.03
Varying value of output power (dbm) in 50 N	0.02 ± 0.004	0.09 ± 0.04	0.06 ± 0.02
Varying value of output power (dbm) in 100 N	0.04 ± 0.004	0.2 ± 0.004	0.11 ± 0.02
Stress (N/mm ²)	0.566	0.579	0.569

The stress for PAB with different diameters was calculated with Equation (1), and is given in Table 2. The stress and output power increased as the PAB diameter decreased. The variation of the output power gradually increased with increasing stress, which indicated a positive relationship that was consistent with Equations (2) and (3). The changing tendencies shown in Figures 7–9 were similar with the stress range from phase M to N in Figure 1. Hence, the theoretical analysis agreed with the experimental results. This indicated that the MB sensor can be used to wirelessly monitor the degradation behavior of PAB.

The Ni and Mo elements of the MB sensor are toxic. However, as shown in Figure 4d, the MB sensor was fully coated with about 10 μm of the quick adhesive and about 15 mm of PLA. The MB sensor was not in direct touch with body tissues during the degradation process. When PAB in the body was fully degraded, a micro-operation was performed to remove the MB sensor. Many papers have used MB sensors in vitro and in vivo to measure and monitor blood coagulation [34] and the host response (wound healing) to an implant in vivo [35]. The sensor has also been applied to monitor the tensile force on sutured wound sites [22] and implanted in a 6 mm femoral segmental defect model

of a rat for non-invasive real-time measurement of the stress [36]. Therefore, the MB sensor was not harmful to the body and was suitable for monitoring the degradation behavior of an implant.

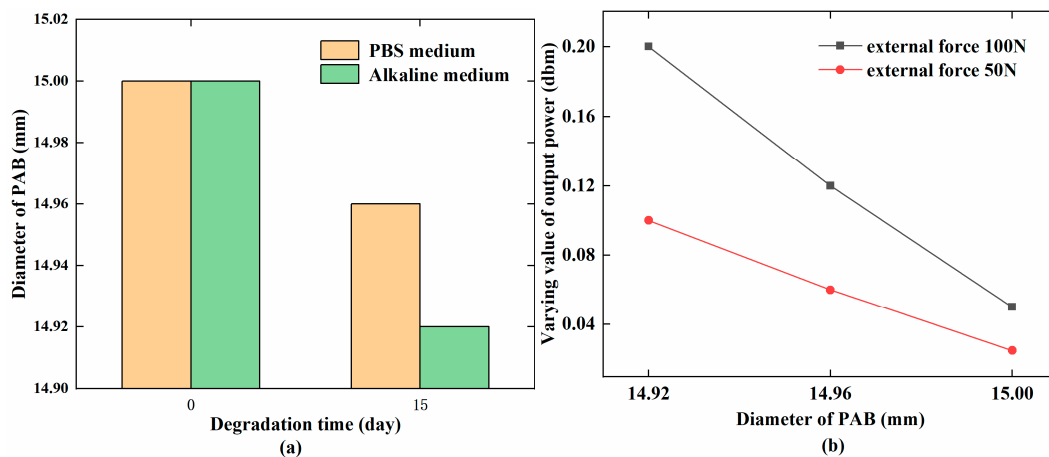


Figure 10. (a) Changes in the PAB diameter (mm) with the degradation time (days); (b) Relationship between the PAB diameter (mm) and varying value of the output power (dbm).

Traditional methods [11,12] are not efficient means of monitoring the degradation behavior if PAB is implanted in the defect site to repair a bone defect. The MB sensor presented for the first time in this study to monitor the degradation behavior of PAB showed innovations in power supply, signal transmission, and data collection. PLA was fully coated on the surface of the MB sensor, which means that it could work without external wires or any batteries to supply power. The signal transmission and the final data are collected by the wireless and passive method which is low cost and does not cause disturbance to the patient, making it convenient to monitor the degradation behavior of PAB in vitro. The results showed that the MB sensor could wirelessly monitor the degradation behavior of PAB in vitro. The MB sensor was smaller in volume and lower in cost [37] than traditional methods. Importantly, biological tissue has almost no effect on the MB sensor, so it could potentially be used in vivo in the future.

5. Conclusions

In this study, a magnetoelasticity-based (MB) sensor was used as a novel method for wirelessly and passively monitoring the degradation behavior of polylactic acid (PLA) artificial bone (PAB). The MB sensor strip was coated with PLA by a 3D printer to form PAB. Hydrolytic degradation of PAB samples was carried out in PBS (pH = 7.4) and NaOH (pH = 12) media over 15 days at 37 °C. The PAB diameter decreased to 14.92 ± 0.02 and 14.96 ± 0.02 mm, respectively. The varying value of the output power changed from 0.04 ± 0.004 dbm to 0.2 ± 0.04 dbm when the PAB diameter was changed from 15 ± 0.05 mm to 14.92 ± 0.02 mm under an external force of 100 N. The monitoring results with the MB sensor coincided with the theoretical analysis. This demonstrates the viability of the MB sensor for monitoring the degradation behavior of PAB in vitro. Importantly, the results showed that biological tissues had no effect on the output value of the MB sensor. There was no need for additional cables or power to collect and transmit the signal for the wireless and passive characteristics of the MB sensor. Importantly, compared with traditional methods (i.e., weight loss and SEM images), the MB sensor was convenient and had low cost to monitor the degradation behavior of PAB in vitro. There are currently many disadvantages that limit the use of this method for monitoring the degradation behavior of PAB in vivo, such as a lack of live animal samples, in vivo PAB implantation process, and related knowledge about transplant operations in vivo. Future research work will involve using the MB sensor to monitor the degradation behavior and rate of PAB in vivo.

Author Contributions: Conceptualization, L.R.; Methodology, Y.T.; Validation, J.W.; Formal analysis, K.Y.; Writing—original draft preparation, K.Y.; Writing—review and editing, Y.T.

Funding: This work is supported in part by the National Natural Science Foundation of China (No. 51405074), and in part by the Natural Science Foundation of Jilin Province (No. 20190201103JC).

Conflicts of Interest: The authors declare no conflict of interest.

References

1. Pihlajamäki, H.; Hirvensalo, E. Poly-L-Lactic of Fractures Pins of Acid Self-Reinforced for Fixation. *Bone Joint J.* **1992**, *74–B*, 853–857.
2. Matsusue, Y.; Nakamura, T.; Iida, H.; Shimizu, K. A long-term clinical study on drawn poly-L-lactide implants in orthopaedic surgery. *J. Long. Term. Eff. Med. Implants* **1997**, *7*, 119–137. [[CrossRef](#)]
3. Ho, Y.-C.; Huang, F.-M.; Chang, Y.-C. Cytotoxicity of formaldehyde on human osteoblastic cells is related to intracellular glutathione levels. *J. Biomed. Mater. Res. B Appl. Biomater.* **2007**, *83*, 340–344. [[CrossRef](#)] [[PubMed](#)]
4. Lu, H.H.; El-Amin, S.F.; Scott, K.D.; Laurencin, C.T. Three-dimensional, bioactive, biodegradable, polymer-bioactive glass composite scaffolds with improved mechanical properties support collagen synthesis and mineralization of human osteoblast-like cells in vitro. *J. Biomed. Mater. Res. Part A* **2003**, *64*, 465–474. [[CrossRef](#)] [[PubMed](#)]
5. Rokkanen, P.U.; Böstman, O.; Hirvensalo, E.; Mäkelä, E.A.; Partio, E.K.; Päätiälä, H.; Vainionpää, S.; Vihtonen, K.; Törmälä, P. Bioabsorbable fixation in orthopaedic surgery and traumatology. *Biomaterials* **2000**, *21*, 2607–2613. [[CrossRef](#)]
6. Middleton, J.C.; Tipton, A.J. Synthetic biodegradable polymers as orthopedic devices. *Biomaterials* **2000**, *21*, 2335–2346. [[CrossRef](#)]
7. Göpferich, A. Mechanisms of polymer degradation and erosion. *Biomaterials* **1996**, *17*, 103–114. [[CrossRef](#)]
8. Mukherjee, D.P.; Pietrzak, W.S. Bioabsorbable fixation: Scientific, technical, and clinical concepts. *J. Craniofac. Surg.* **2011**, *22*, 679–689. [[CrossRef](#)]
9. Cooper, J.A.; Lu, H.H.; Ko, F.K.; Freeman, J.W.; Laurencin, C.T. Fiber-based tissue-engineered scaffold for ligament replacement: Design considerations and in vitro evaluation. *Biomaterials* **2005**, *26*, 1523–1532. [[CrossRef](#)]
10. Ouyang, H.W.; Goh, J.C.H.; Mo, X.M.; Teoh, S.H.; Lee, E.H. The efficacy of bone marrow stromal cell-seeded knitted PLGA fiber scaffold for Achilles tendon repair. *Ann. N. Y. Acad. Sci.* **2002**, *961*, 126–129. [[CrossRef](#)]
11. Tsuji, H.; Ikada, Y. Properties and morphology of poly(L-lactide) 4. Effects of structural parameters on long-term hydrolysis of poly(L-lactide) in phosphate-buffered solution. *Polym. Degrad. Stab.* **2000**, *67*, 179–189. [[CrossRef](#)]
12. Yuan, X.; Mak, A.F.T.; Yao, K. Surface degradation of poly (L-lactic acid) fibres in a concentrated alkaline solution. *Polym. Degrad. Stab.* **2003**, *79*, 45–52. [[CrossRef](#)]
13. Shih, C. Chain-end scission in acid catalyzed hydrolysis of poly (D,L-lactide) in solution. *J. Control. Release* **1995**, *34*, 9–15. [[CrossRef](#)]
14. Iwata, T.; Doi, Y. Morphology and Enzymatic Degradation of Poly (L-lactic acid) Single Crystals. *Macromolecules* **1998**, *9297*, 2461–2467. [[CrossRef](#)]
15. Soller, B.R.; Zhang, S. Optical measurement of tissue pH for surgical and critical care monitoring. In Proceedings of the BiOS '98 International Biomedical Optics Symposium, San Jose, CA, USA, 23–24 January 1998; Volume 3259, pp. 122–129.
16. Ohman, H.; Vahlquist, A. In vivo studies concerning a pH gradient in human stratum corneum and upper epidermis. *Acta Derm. Venereol.* **1994**, *74*, 375–379. [[PubMed](#)]
17. Prince, S.; Malarvizhi, S. Analysis of spectroscopic diffuse reflectance plots for different skin conditions. *Spectroscopy* **2010**, *24*, 467–481. [[CrossRef](#)]
18. Tannock, I.F.; Rotin, D. Acid pH in Tumors and Its Potential for Therapeutic Exploitation Perspectives in Cancer Research Acid pH in Tumors and Its Potential for Therapeutic Exploitation. *Cancer Res.* **1989**, *49*, 4373–4384.

19. Sims, C.; Seigne, P.; Menconi, M.; Monarca, J.; Barlow, C.; Pettit, J.; Puyana, J.C. Skeletal muscle acidosis correlates with the severity of blood volume loss during shock and resuscitation. *J. Trauma* **2001**, *51*, 1137–1145, discussion 1145–1146. [[CrossRef](#)] [[PubMed](#)]
20. Lin, M.H.; Anderson, J.; Pinnaratip, R.; Meng, H.; Konst, S.; DeRouin, A.J.; Rajachar, R.; Ong, K.G.; Lee, B.P. Monitoring the Long-Term Degradation Behavior of Biomimetic Bioadhesive Using Wireless Magnetoelastic Sensor. *IEEE Trans. Biomed. Eng.* **2015**, *62*, 1838–1842. [[CrossRef](#)] [[PubMed](#)]
21. Tan, Y. A Passive and Wireless Sensor for Bone Plate Strain Monitoring. *Sensors* **2017**, *17*, 2635. [[CrossRef](#)]
22. De Rouin, A.; Pacella, N.; Zhao, C.; An, K.N.; Ong, K.G. A wireless sensor for real-time monitoring of tensile force on sutured wound sites. *IEEE Trans. Biomed. Eng.* **2016**, *63*, 1665–1671. [[CrossRef](#)] [[PubMed](#)]
23. Ueno, T.; Qiu, J.Q.J.; Tani, J. Magnetic force control based on the inverse magnetostrictive effect. *IEEE Trans. Magn.* **2004**, *40*, 1601–1605. [[CrossRef](#)]
24. Polanschiütz, W. Inverse magnetostrictive effect and electromagnetic destructive testing methods. *NDT Int.* **1986**, *19*, 249–258. [[CrossRef](#)]
25. Modzelewski, C.; Savage, H.T.; Kabacoff, L.T.; Clark, A.E. Magnetomechanical coupling and permeability in transversely annealed metglas 2605 alloys. *IEEE Trans. Magn.* **1981**, *17*, 2837–2839. [[CrossRef](#)]
26. O’Handley, R.C. *Modern Magnetic Materials: Principles and Applications*; Wiley-Interscience: New York, NY, USA, 2000; ISBN 0471155667.
27. Wun-Fogle, M.; Savage, H.T.; Clark, A.E. Sensitive, wide frequency range magnetostrictive strain gage. *Sens. Actuators* **1987**, *12*, 323–331. [[CrossRef](#)]
28. Ren, L.; Yu, K.; Tan, Y. Wireless and Passive Magnetoelastic-Based Sensor for Force Monitoring of Artificial Bone. *IEEE Sens. J.* **2019**, *19*, 2096–2104. [[CrossRef](#)]
29. Barandiaran, J.M.; Gutierrez, J.; Gómez-Polo, C. New sensors based on the magnetoelastic resonance of metallic glasses. *Sens. Actuators A Phys.* **2000**, *81*, 154–157. [[CrossRef](#)]
30. Narita, F.; Fox, M. A Review on Piezoelectric, Magnetostrictive, and Magnetoelectric Materials and Device Technologies for Energy Harvesting Applications. *Adv. Eng. Mater.* **2018**, *20*, 1–22. [[CrossRef](#)]
31. Hafezi, H.; Robertson, T.L.; Moon, G.D.; Au-Yeung, K.Y.; Zdeblick, M.J.; Savage, G.M. An ingestible sensor for measuring medication adherence. *IEEE Trans. Biomed. Eng.* **2015**, *62*, 99–109. [[CrossRef](#)]
32. Navarro, M.; Ginebra, M.P.; Planell, J.A.; Barrias, C.C.; Barbosa, M.A. In vitro degradation behavior of a novel bioresorbable composite material based on PLA and a soluble CaP glass. *Acta Biomater.* **2005**, *1*, 411–419. [[CrossRef](#)]
33. Araque-Monrós, M.C.; Vidaurre, A.; Gil-Santos, L.; Gironés Bernabé, S.; Monleón-Pradas, M.; Más-Estellés, J. Study of the degradation of a new PLA braided biomaterial in buffer phosphate saline, basic and acid media, intended for the regeneration of tendons and ligaments. *Polym. Degrad. Stab.* **2013**, *98*, 1563–1570. [[CrossRef](#)]
34. Puckett, L.G.; Barrett, G.; Kouzoudis, D.; Grimes, C.; Bachas, L.G. Monitoring blood coagulation with magnetoelastic sensors. *Biosens. Bioelectron.* **2003**, *18*, 675–681. [[CrossRef](#)]
35. Vlaisavljevich, E.; Holmes, H.R.; Tan, E.L.; Qian, Z.; Trierweiler, S.; Ong, K.G.; Rajachar, R.M. Magnetoelastic vibrational biomaterials for real-time monitoring and modulation of the host response. *J. Mater. Sci. Mater. Med.* **2013**, *24*, 1093–1104. [[CrossRef](#)]
36. Klosterhoff, B.S.; Ghee Ong, K.; Krishnan, L.; Hetzendorfer, K.M.; Chang, Y.-H.; Allen, M.G.; Guldborg, R.E.; Willett, N.J. Wireless Implantable Sensor for Noninvasive, Longitudinal Quantification of Axial Strain Across Rodent Long Bone Defects. *J. Biomech. Eng.* **2017**, *139*, 111004. [[CrossRef](#)] [[PubMed](#)]
37. Ee, L.T.; Pereles, B.D.; Horton, B.; Shao, R.; Zourob, M.; Keat, G.O. Implantable biosensors for real-time strain and pressure monitoring. *Sensors* **2008**, *8*, 6396–6406. [[CrossRef](#)]

